Faster methods for estimating arc centre position during VAR and results from Ti-6Al-4V and INCONEL 718 alloys

Gopinathan Nair, Bindu; Winter, N; Daniel, B; Ward, Mark

DOI:
10.1088/1757-899X/143/1/012012

Faster methods for estimating arc centre position during VAR and results from Ti-6Al-4V and INCONEL 718 alloys

2016 IOP Conf. Ser.: Mater. Sci. Eng. 143 012012

(http://iopscience.iop.org/1757-899X/143/1/012012)

Faster methods for estimating arc centre position during VAR and results from Ti-6Al-4V and INCONEL 718 alloys

B G Nair[1], N Winter[2], B Daniel[3], R M Ward[1]
[1] Metallurgy & Materials, University of Birmingham, Birmingham, B15 2TT, UK
[2] Timet, Witton, Birmingham, UK, [3] Special Metals, Hereford UK

E-mail: r.m.ward@bham.ac.uk

Abstract. Direct measurement of the flow of electric current during VAR is extremely difficult due to the aggressive environment as the arc process itself controls the distribution of current. In previous studies the technique of "magnetic source tomography" was presented; this was shown to be effective but it used a computationally intensive iterative method to analyse the distribution of arc centre position. In this paper we present faster computational methods requiring less numerical optimisation to determine the centre position of a single distributed arc both numerically and experimentally. Numerical validation of the algorithms were done on models and experimental validation on measurements based on titanium and nickel alloys (Ti6Al4V and INCONEL 718). The results are used to comment on the effects of process parameters on arc behaviour during VAR.

1. Introduction

Presently Vacuum Arc Remelting (VAR) is the most commonly used melting process for the manufacture of high quality segregation-free ingots of titanium and nickel alloys. Due to the stringent targets for the properties of these materials in demanding applications, the process is continuously enhanced to produce these alloys with excellent homogeneity and purity [1]. In VAR the electrode is melted by a plasma arc, however the distributions of heat, current and mass flux within the 'arc' (or 'arcs') are not directly controlled. Studies have shown a time-varying, asymmetry in the distribution of arc current which could affect the velocity and temperature distributions in the melt pool [2]. Ward et al. [3] reported an ensemble arc motion with the time averaged position of maximum current flow, which potentially limits the validity of a 2-D axisymmetric modelling concept of VAR [4]. Due to the aggressive environment some indirect methods of measurement based on voltage gradient on the crucible walls and measurement of magnetic flux surrounding the crucible have been previously proposed [5] to better understand the distribution of current within the process. Woodside et al. [6] reported observing several arc distribution modes during production of Ti6Al4V that could impact solidification times.

The technique of magnetic source tomography (MST) is capable of estimating the locations of multiple centres of current density simultaneously, based on measurements of magnetic flux density outside the crucible. As originally proposed this technique used an optimisation routine based on the Biot Savart Law (BSL-MST algorithm) [7-8]. Due to the computationally intense nature of the BSL-MST algorithm, however, faster methods are appealing. In this paper we present two computationally efficient and faster optimisation algorithms to supplement the BSL-MST method, using Ampere's Law (AL-MST algorithm) and Neural networks (NN-MST), to determine the centre position of a single distributed arc. Numerical validations of the algorithms were done on models developed using a commercial finite element electromagnetic code (Opera 3d).

Experimental studies were based on melts of titanium and nickel alloys (Ti-6Al-4V and INCONEL 718), interpreting measurements of magnetic field, arc voltage and current together with process video. The results from the algorithms are compared and are used to comment on the effects of process parameters on arc behaviour during VAR. In particular, the link between arc behaviour and the growth and re-melting of the solid skin at the ingot edge is explored.

2. Theory

Patterns of current distribution during VAR and the expected resultant magnetic field from off-centre current flow are shown in figure 1(*a*)–(*c*) (from [7]). In VAR the current is not deliberately injected at known locations; instead the arc process itself controls the location of the current, and the passive sensors and reconstruction algorithm are used to determine its spatial distribution. Magnetically silent distributions of current (e.g. in which the current flow through the crucible and its return through the ingot are

axisymmetric) do not produce a measurable magnetic field outside the crucible and therefore cannot be reconstructed. However, if either of these flows deviates from axisymmetry, an external field is produced. Such deviations are likely to be caused by drip shorts, by a constricted arc away from the ingot centre line and even by a diffuse arc if not perfectly centred. The term 'arc centre location', often shortened to 'arc location' in this paper, refers to the position of the centre of a locally-axisymmetric distribution of current between the electrode base and ingot top.

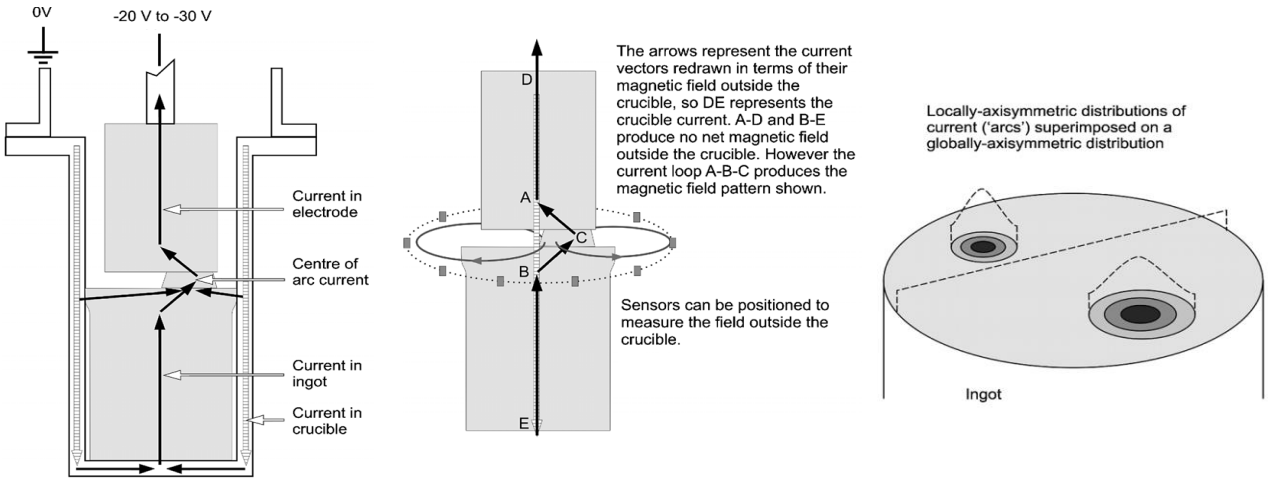

(a) (b) (c)

Figure 1**.** Magnetic fields during VAR. The techniques presented in this paper are to estimate the centre positions and additional currents of off-centre arcs by using measurements of magnetic field outside the crucible. (a) The current paths during VAR and the B field due to an off-centre arc. (b) The current paths redrawn in terms of their field outside the crucible, and the field due to an off-centre arc. (c) Suggested distribution of current during VAR consisting of a globally axisymmetric background current (the diffuse arc), with locally axisymmetric current flows ('arcs') superimposed. Details can be found in [7].

3. Magnetic Source Tomography – Three approaches

3.1.MST using Biot Savart Law (BSL – MST)

Assuming that the currents are varying slowly enough that the system can be considered to be magnetostatic, the magnetic flux density *B* arising from current density *J* in volumes d*v* can be calculated using the Biot–Savart law shown in equation (1),

$$B(r) = \frac{\mu_o}{4\pi} \int J(r') \times \frac{r-r'}{|r-r'|^3} dv' \qquad (1)$$

where μ_0 is the permeability of free space and also of nonmagnetic objects, *r* is the vector from the origin to the measurement point, *r'* is the vector from the origin to field point and *J*(*r'*) is the current density at *r'*. We considered that the materials used in the important parts of the systems in this paper (Ti6Al4V, INCONEL 718 and copper) had μ_r=1. In BSL-MST, the magnetic field created outside the crucible due to an arc centre at an arbitrary location was represented as a linear interpolation between the *B* fields resulting from arcs at points on a square grid surrounding the true arc location. Despite the nonlinearity in the underlying equations, given a sufficiently fine grid (1 cm in this case) sufficiently accurate results were obtained. Simulations were performed to make the array of *B* field values corresponding to arcs at these grid points using the finite element software Opera 3D. Constrained nonlinear optimization was used to estimate the currents and centre locations of a fixed number of arcs using the results from the forward models, so that the predicted B fields outside the furnace matched most closely with the measurements at a given time. A key assumption is that superposition applies when calculating the total field from current split into multiple arcs. Further details of BSL – MST are reported in [6-7].

3.2. MST using Amperes Law (AL – MST)

This method uses 2-D calculations assuming that the furnace can be represented as an infinitely-long crucible and a single off-centre arc, both carrying current and both creating magnetic field which can be measured at sensors outside. Neither of them necessarily carry the total process current, as any current that is co-axial in both of them will produce fields which cancel to zero outside. Each sensor is used to estimate

the arc centre position from its $B_{x,\ y}$ readings, I_C , and I_A, and the algorithm then chooses I_C and I_A parameters to make all the sensors estimate the arc to be at the same location as far as possible. This approach is also magnetostatic and uses Ampere's law by inverting it so that, given knowledge of I_C , I_A and the position of the crucible current (0,0) , the position of the arc current can be calculated :

$$\oint H.dl = I_{enc} \quad (2)$$

It was found that choosing the I_C and I_A parameters to solely place the arc position estimates as close together as possible led to significant errors in the position estimation; the following cost function was found to be better, which favours solutions that minimise I_C and I_A as well as putting the arc position estimates close together:

$$\overline{D_i} * \sqrt{I_C^2 + I_A^2} \quad (3)$$

where I_C - Crucible current, I_A - Arc current, D_i – distance from the arc position estimate from an individual sensor *i* to its average from all sensors.

3.3. MST using Neural Network (NN – MST)

Various nonlinear connectionist model architectures (in the Matlab Neural Network Toolbox) were tested as a means of predicting the centre location of a single arc based on the external *B* measurements. Using either modelled or experimental datasets, 70% of the data was used to train the neural network, 15 % was used for validation and the final 15% for testing. A neural network using Bayesian regularisation was finally selected due its performance when testing the network. The network was initially trained using arc centre models positioned on a 2 cm x 2 cm x 2 cm grid, and expected to interpolate at points between these. One advantage of neural networks over e.g. K-nearest neighbours is that once a network has been trained it can predict the arc locations quickly due to being a direct computation, without searching at run-time. However it is important to note that, as this is a purely data-driven approach that doesn't directly contain the process physics, it is likely to be poor at extrapolating beyond the domain of the training data. As an example, it was found necessary to deliberately add noise to the training data in order for the network to be able to function well on noisy test data.

4. Experimental methods

4.1. Ti6Al4V : Magnetic field measurements were done on a first melt experiment in which an electrode was melted into a crucible of 0.66 m diameter at a higher current (than used for INCONEL 718). To gather the magnetic field data two rings of ten sensor boxes each containing 3 axis Hall effect sensors (measuring azimuthal, radial and axial flux density) were mounted at heights 1.075m and 1.475 m from the base plate on a 1.06 m diameter circle, outside the furnace cooling jacket. The outputs from the sensors were measured using National Instruments differential amplifier and 10 kHz low pass filter at a 1 KHz sampling rate. Video recordings were made for the whole melt using standard video cameras at 25 frames per sec.

4.2. INCONEL 718 : Magnetic field data were gathered during VAR of an ingot of INCONEL 718. The experiment was done at 6 kA, from 0.42 m / 0.22 m electrode into a 0.508 m diameter mould [3]. Twelve sensor boxes each containing 3 axis Hall effect sensors were mounted in a ring on the crucible inside the water jacket. The outputs from the sensors were measured using National Instruments differential amplifiers and 10 kHz low pass filter at a 5 KHz sampling rate.

In both cases the measurements of magnetic field were compensated using their mean value, owing to the uncertainty in the zero-field output of the Hall sensors used here. Additionally for the Ti-6Al-4V experiment the z-components of measured field were compensated for the effects of the solenoid stirring coil used.

5. Results

5.1. Validation and performance analysis of the algorithms using simulated data

The algorithms were first tested on simulated data, in which the arc location and B field were known. In all cases the prediction of arc position became more accurate as the amount of simulated noise was reduced, following the trends shown in [7]. The results of trying to locate arcs in the plane of, and 10 cm above, the sensors are shown below (figure 2) for the case when the simulated external B values used had no noise added. (The results for arcs below the sensors were equivalent to those above them). The disks represent cross sections through the plane between the electrode and ingot for a simulation of IN718 VAR, and the colour at each point represents the position error found when attempting to locate a single arc that had been placed at that point.

Good performance was found for BSL-MST, with only a few points on either plane in which the estimated position errors were above 8 cm. AL-MST was found to be effective when the sensors were at the same plane as the arc. However its accuracy decreased strongly when the arc was above or below the sensors, particularly as the arc was closer to the edge of the electrode; this may relate to the truly 3-dimensional nature of the current flow which is being modelled here as purely 2-d. (Although not shown here, AL-MST became increasingly poor at greater vertical displacements, whereas e.g. BSL-MST was able to work at 35 cm vertical difference.) Finally NN-MST was found to be reasonably accurate regardless of the sensor position relative to the arc, and this may be improved by further refinement in the choice of training data and method.

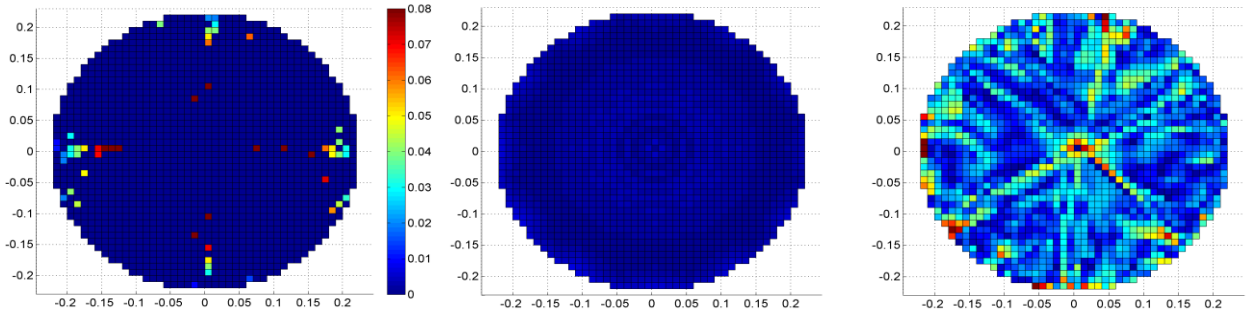

BSL-MST; Sensors in the arc plane | AL-MST; Sensors in the arc plane | NN-MST; Sensors in the arc plane

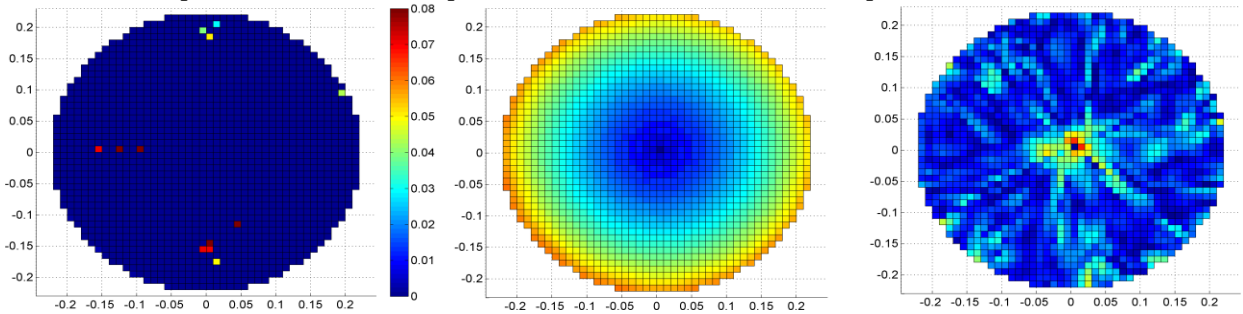

BSL-MST; Sensors above the arc plane | AL-MST; Sensors above the arc plane | NN-MST; Sensors above the arc plane

Figure 2. Arc location error from INCONEL 718 VAR model data. The colour at a point represents the error in m when using a particular algorithm to locate an arc placed there from the simulated magnetic field measurements outside the furnace.

Programmed in Matlab on an Intel Core i7 processor @3.4 GHz, BSL-MST took 1.2 sec to analyse the arc centre position for a single set of B field measurements (probably too slow for real-time use), whereas AL-MST required only 0.017 sec. However NN-MST could analyse an entire melt data set – nearly 300k results from 8 hours at 10 Hz - in less than 2 s in total once it had been trained.

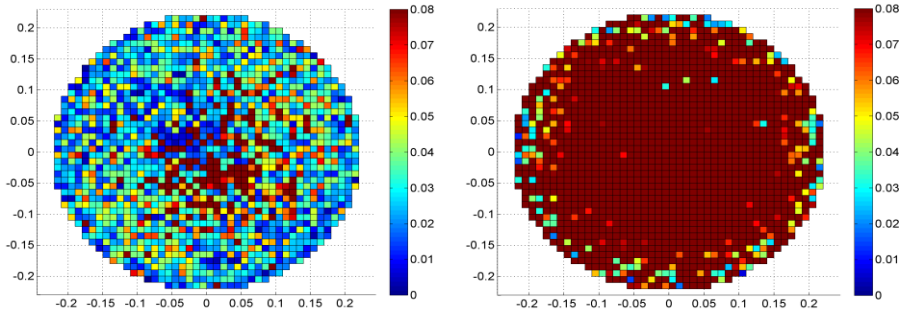

10 sensors | 5 sensors

Figure 3. Ti6Al4V model, Position error computed using BSL – MST algorithm with 10 and 5 sensors

The number of sensors used was also found to be important. In previous work [7] it was suggested that 8 sensors was the minimum needed for accurate arc location given typically noisy measurements. In figure 3 the results of trying to locate arcs in the plane of the sensors in a simulated Ti-6Al-4V melt with

SNR of 40 dB are shown using 10 and 5 sensors; it can be seen that the position errors were large when using only 5 sensors. Ideally, for industrial use, a very small number of sensors would be required (e.g. 2 at each height), but these results imply that more would be preferred.

5.2. Physical experiments

5.2.1 Determination of Arc centre position. Figure 4 shows video from a first melt Ti6Al4V trial superimposed with the magnetic measurements. The results from the upper ring are shown with a smaller radius in the figure. The size & direction of the cones represent the magnitude and direction of the B fields measured by each sensor. In this time range the ingot top is closer to the bottom set of sensors; hence the B field is stronger there compared to that at the upper sensors. Note that the numerical values of the B field are not shown but the scaling is constant between frames. The red line in the middle shows the direction of the solenoid current (up=+ve, down=-ve). The arc centre positions computed by the algorithms are shown as 3 dots, using the readings from the lower set of sensors. The yellow and cyan dots are the arc centres computed by BSL-MST and AL-MST and the green dot is from the neural network . It can be seen that the arc centre positions match well even when computed using different techniques.

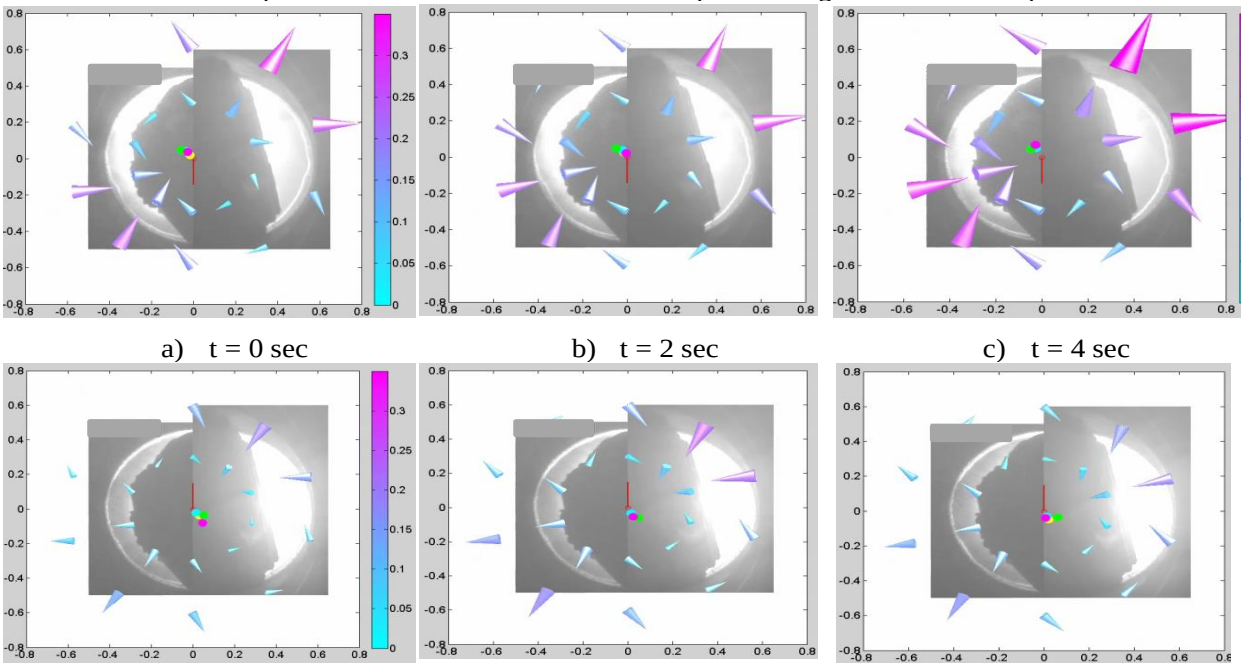

a) t = 0 sec b) t = 2 sec c) t = 4 sec

d) t = 6 sec e) t = 8 sec f) t = 10 sec

Figure 4. Representations of magnetic flux, arc centre and solenoid current at 2 sec intervals during a trial first melt of Ti-6Al-4V

Between figures 4 (a-c) the estimated arc position makes a slight movement corresponding with the variations in the magnetic field. A similar trend is observed in figures 4 (d-f). However when the solenoid current changes direction between fig 4 c and fig 4 d, the estimated arc position makes a larger move corresponding with a large change in the measured magnetic field values. Results from VAR of INCONEL 718 have been shown in previous work e.g. [3, 5].

A difference in arc behaviour during VAR was observed between Ti-6-4 and IN 718. The angle of rotation of the arc centre around the ingot centreline was plotted versus time and is shown in figure 5 for sections of melts of both alloys. It can be seen that for this Ti-6-4 first melt (5 a) the arc position was mostly at around 0 radians when the solenoid current was +ve or +/- 3 radians (180°) when it was –ve. (Although these positions are not fixed; some variation can be seen between 0-200 s and 1300-1500 s). For IN 718 (5 b), however, the arc was observed to rotate fairly continuously around the ingot centreline, reversing direction at random times. This can be seen by the arc position azimuth continuously increasing or decreasing versus time.

The difference between these two VAR experiments can also be seen in figure 6, in which the distributions of current at the estimated arc centre location in the x-y plane over time are shown. Most of the current is carried by arc centres near the edge of the electrode in IN 718 VAR, but by arc centres near the electrode centre in Ti-6-4. (Note that it is not possible to measure the radius of a symmetrical arc

current distribution from external measurements, however. So the current could have been almost uniformly distributed over the whole electrode bottom in the Ti-6-4 experiment, with just the centre of the distribution moving slightly in response to the solenoid current). It's not clear whether the arc centre being found close to the ingot centre in Ti-6-4 VAR is compatible with the variations in brightness seen as it moves around; it would be expected that, the further the arc centre from the ingot centre, the greater the variations in brightness that would be observed. However the fact that the algorithm used here is able to estimate the *z* position of the arc (and hence the ingot top) reasonably accurately suggests that it should also be getting *x* and *y* correct.

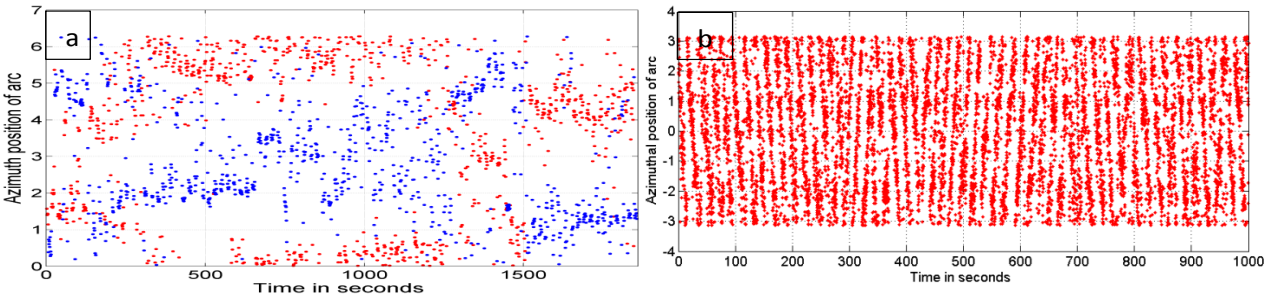

Figure 5. Azimuthal position of the estimated arc location versus time for a)Ti-6Al-4V(where red is used to indicate measurement points for which the solenoid current was positive),b) IN 718

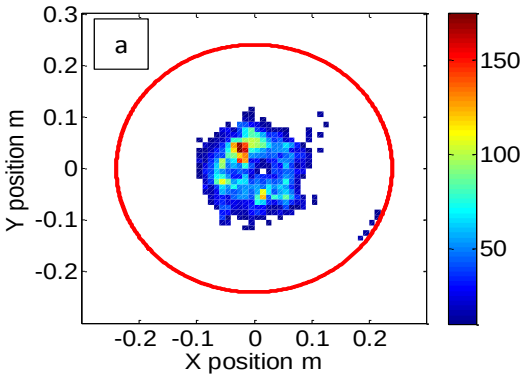

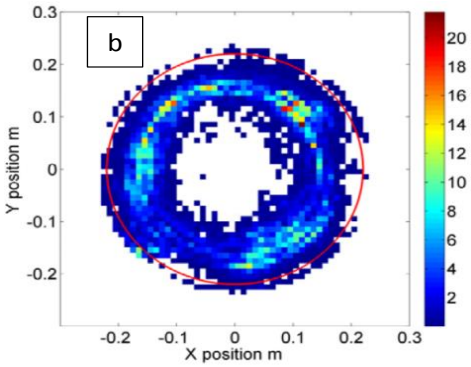

Figure 6. The distribution of current carried by arc centre positions from BSL-MST in terms of A/m^2 for a) Ti6Al4V, b) IN718

The differences between IN718 and Ti-6-4 may be related to the drip shorts that occur frequently in typical Ni superalloy VAR, causing arcs continually re-start near the edge of the electrode; these are typically not present in Ti-6-4 VAR due to the higher currents and larger gaps used. The influence of current on drip shorts has been investigated in depth by Zanner and co-authors (e.g. the authors of [9]). However, Woodside et al. [6, fig 7] have interpreted magnetic field data to give final-melt Ti-6-4 VAR arc centre position distributions close to the edge of the electrode as well as near the centre, and they attributed the differences to electrode preparation.

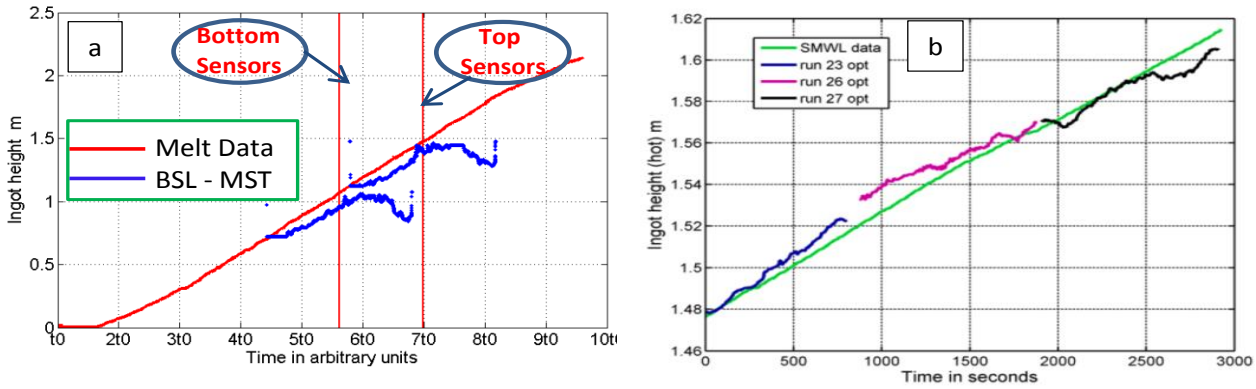

Figure 7. Estimation of the ingot top position using BSL –MST, from a) Ti6Al4V and b) IN 718 melt

5.2.2. Estimation of Ingot top position. The z coordinates from the BSL-MST arc position algorithm were also investigated. They are shown plotted versus time in figure 7, compared with the ingot top position from the melt data. For the titanium alloy example, it is seen that once the ingot top had moved past the sensor rings, the algorithm didn't estimate its position well. However the algorithm behaved reasonably well for the nickel alloy irrespective of whether the ingot top was above or below the sensors.

To investigate this, 2-arc noise-free models of the production of Ti6Al4V and INCONEL718 were produced and the likely estimated arc location errors were calculated using the BSL- MST algorithm. The results are shown in figure 8 (a-b) when the ingot top was 10 cm above the sensors. It can be seen that the errors were greater for the Ti-6-4 furnace simulation. This may be due to the sensors being much closer to the ingot in the IN 718 simulation, corresponding to their physical placement inside the furnace water jacket in this case, as opposed to being outside the cooling jacket for Ti-6-4.

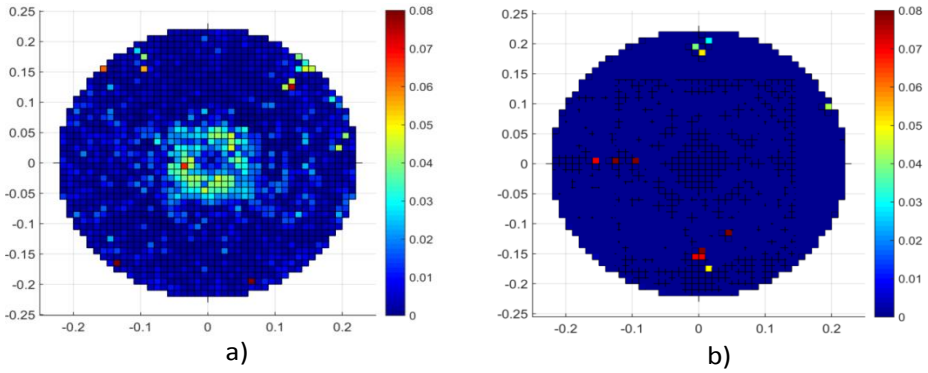

Figure 8. Position error when ingot top is 10 cm above the sensor for models a) Ti6Al4V, b) INCONEL 718

5.2.3. Effects on solidification. The spatial distribution of heat, current and mass flux on the ingot top will affect the solidification during VAR [9]. The size of the effect may be significant, or not, depending on the conditions; it could influence the thickness of the layer needing to be machined off, the creation of chemical segregation, and the formation of surface irregularities for example.

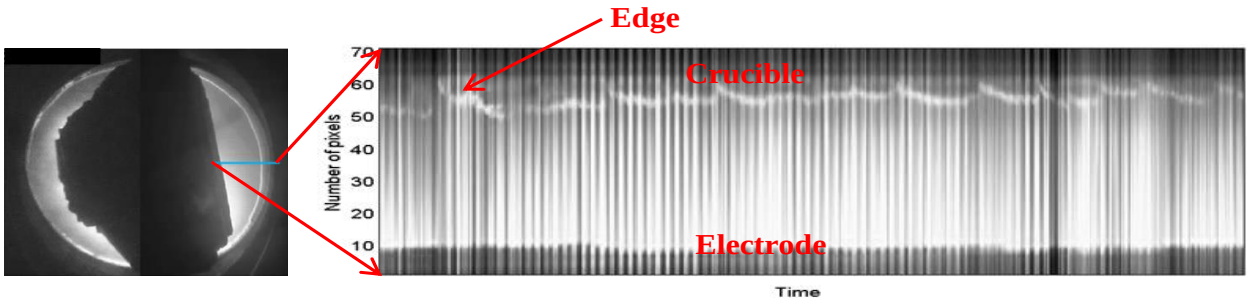

Figure 9: Local brightness and edge thickness over 31 min from a first melt VAR of Ti6Al4V

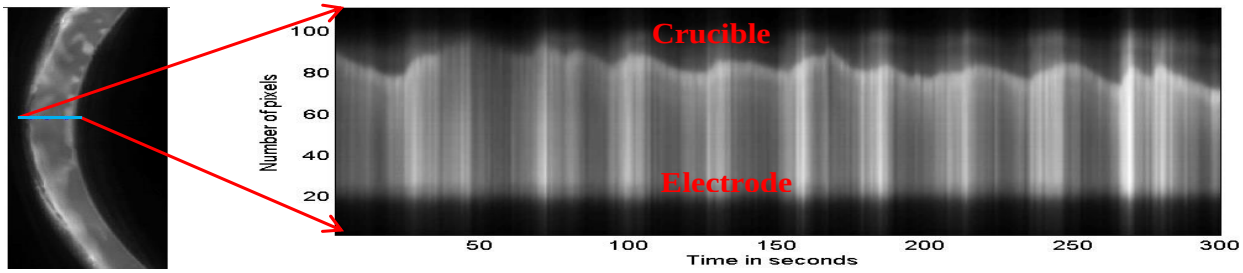

Figure 10: Local brightness and edge thickness over 5 min from a first melt VAR of INCONEL 718

As the arc current flux should correlate with the visible intensity of reflected light, the correlation between the thickness of the solid material at the edge of the ingot and the local brightness was

investigated. (The word 'edge' has been used to describe the solid thickness here, as 'shelf' has a specific meaning for Ni superalloys referring to features possibly beneath the top surface.) Some results from the Ti-6-4 first melt are shown in figure 9. It can be seen that the edge thickness does vary over time, but not in direct relation to the local instantaneous brightness. Corresponding results are shown from VAR of an IN718 electrode in figure 10. Here it can be seen that there is significant growth and recession of the solid region at the edge of the ingot during most periods of brighter and darker reflected light, with recession happening when the light is brighter, presumably due to increased heat flux.

The difference between the results from Ti-6-4 and IN718 may be due to the observation that the arc centre location was much closer to the electrode (and ingot) edge during the VAR of IN718 than in Ti-6-4; this would presumably have increased the magnitude of the increase and decrease in local heat and current flux for IN718. The authors thank a referee for the observation that "…for Ti-6Al-4V VAR … At intermediate gaps, it is entirely possible to have the bulk of the arc centered under the electrode but still see arc light intensity rotation in the annulus that correlates with stirring field direction. These variations may not be strong enough to melt back shelf formed at the ingot-crucible interface…". However the ingot edge during Ti-6-4 VAR is still likely to be affected by axisymmetry over time in the arc or ingot/mold heat transfer, coupled with the effects of MHD in the large liquid pool volume at high overall current.

6. Conclusion

Faster optimisation algorithms have been developed to estimate the position of the centre of the magnetic centre of the arc current in vacuum arc remelting using magnetic source tomography. The algorithms were validated and compared with numerical models, and then applied to magnetic field measurements from trial VAR melts of titanium and nickel alloys. The slowest algorithm (BSL-MST) was found to perform well on simulated data and also to be able to correctly predict the ingot top position from experimental data. The quicker methods AL-MST and NN-MST were 2-4 orders of magnitude faster than BSL-MST in the implementation here (Matlab), with varying result quality. A strong link between instantaneous arc behaviour and the growth and re-melting of the solid skin at the ingot edge was observed for the nickel superalloy VAR ingot, but for Ti-6-4 the relationship was more complex although growth and recession were still observed; this may be linked to the arc centre position being typically interpreted as close to the electrode centre for the Ti-6-4 melt presented here but close to the electrode edge for IN718.

7. Acknowledgements

Dr Ward and Dr Nair are grateful for financial support from TIMET for this work; to Andrew Wilson at TIMET Witton for providing process data; and to Drs Matthew Thomas (Witton) and Ashish Patel (Morgantown) for support.

8. References

[1] Zanner F J and Bertram L A 1985 Vacuum Arc Remelting – An Overview Proc.8th Int. Conf. Vac. Metall. 512-522
[2] Shevchenko D M and Ward R M 2007 Liquid metal pool behaviour during the VAR of INCONEL 718 *Proc. Int. Symp. Liquid Metal Processing and Casting* 25-30
[3] Ward R M, Daniel B and, Siddall R J 2005 Ensemble arc motion and solidification during the vacuum arc remelting of a nickel-based superalloy *Proc. Int. Symp. Liq. Met Proc.Cas.*
[4] Koulis P, Djambazov G, Ward R M, Yuan L and Lee P D 2013 A multi-scale 3D model of the vacuum arc remelting process *Metallurgical and Materials Transactions A* **44A** 5365 – 5376
[5] Ward R M and Jacobs M H 2004 Electrical and magnetic techniques for monitoring arc behaviour during VAR of INCONEL 718 : Results from different operating conditions *Journal Mat. Sci.* **39** 7135-7143
[6] Woodside C R, King P E and Nordlund C 2013 Arc distribution during the vacuum arc remelting of T-6Al- 4V *Metallurgical and Materials Transactions B* **44B** 154 -165
[7] Nair B G and Ward R M 2009 An analysis of the use of magnetic source tomography to measure the spatial distribution of electric current during vacuum arc remelting *Meas. Sci. Technol.* **20** 045701
[8] Nair B G and Ward R M 2009 3-D analysis of magnetic field to monitor arc current during vacuum arc remelting *Proc. Int. Symp. Liquid Metal Processing and Casting*
[9] Williamson R L, Schlienger M E, Hysinger C I and Beaman J J 1997 Modern control strategies for vacuum arc remelting of segregation sensitive alloys *Superalloys 718,625,706 and various derivatives* 37 -46